BIOLOGICALLY DERIVED NANOPARTICLE ARRAYS VIA A SITE-SPECIFIC RECONSTITUTION OF FERRITIN AND THEIR ELECTROCHEMISTRY

Jae-Woo Kim[a*], Sang H. Choi[b], Peter T. Lillehei[b], Glen C. King[b], James R. Elliott[c], Sang-Hyon Chu[d], Yeonjoon Park[a], and Gerald D. Watt[e],

[a] Science and Technology Corporation, Hampton, VA 23666;
[b] AMPB, NASA Langley Research Center, Hampton, VA 23681-2199;
[c] AAB, NASA Langley Research Center, Hampton, VA 23681-2199;
[d] National Institute of Aerospace, Hampton, VA 23666;
[e] Department of Chemistry, Brigham Young University, Provo, UT 84602

ABSRACT

Nanoparticle arrays biologically derived from an electrochemically-controlled site-specific biomineralization were fabricated on a gold substrate through the immobilization process of biomolecules. The work reported herein includes the immobilization of ferritin with various surface modifications, the electrochemical biomineralization of ferritins with different inorganic cores, the fabrication of self-assembled arrays with the immobilized ferritin, and the electrochemical characterization of various core materials. Protein immobilization on the substrate is achieved by anchoring ferritins with dithiobis-N-succinimidyl propionate (DTSP). A reconstitution process of electrochemical site-specific biomineralization with a protein cage loads ferritins with different core materials such as Pt, Co, Mn, and Ni. The ferritin acts as a nano-scale template, a biocompatible cage, and a separator between the nanoparticles. The nano-sized metal-cored ferritins on a gold substrate displayed a good electrochemical activity for the electron transport and storage, which is suitable for bioelectronics applications such as biofuel cell, bionanobattery, biosensors, etc.

Keywords: Ferritin, immobilization, site-specific reconstitution, biomineralization, and bioelectronics

INTRODUCTION

Long-duration human space exploration requires enabling technologies that offer solutions to many real and potential challenges as listed in NASA's Bioastronautics Critical Path Roadmap (BCPR).[1] The human body is an extraordinary and complicated system that automatically detects and responds to dramatic environmental changes.[1,2] As one system in the body changes, this change brings other changes in other systems throughout the body, resulting in complex changes. Each problem area needs to be monitored using sensors and treated by any cure mechanisms. These in-vivo sensing and cure modules that would provide in-situ and accurate sensing and treatment capability require miniaturized and biocompatible power source. Biological and medical problems occurring during space missions, in fact, are closely related to many of the health issues on Earth. One

* Electrochemical Society Active Member, e-mail: fn.j.kim@larc.nasa.gov.

critical change in astronaut body is significant reduction in muscle mass and strength after long-duration space flight.[2]

To be minimally invasive sensors combined with power generation and energy storage devices to monitor health condition, system miniaturization and compact integration are equally important. Various inorganic molecules appear to be good candidates as an energy storage and generation materials. If they are easily incorporated into biological molecules by employing bioinorganic chemistry techniques, a basic power unit can be formed in such a small scale and ensure biocompatibility. The ferritin used in this work is a natural iron storage protein that presents a high degree of structural similarity across a wide range of biological species.[3] The ferritin molecule shown in Fig. 1 is composed of 24 organic subunits that build a segmented hollow protein shell with an outer diameter of 12.5 nm and an inner diameter of 7.5 nm. The mineral core of naturally existing ferritins is composed of an antiferromagnetic iron oxide (ferrihydrite) within its hollow and spherical protein interior. The assembled structure of ferritin is remarkably stable and robust, and able to withstand biologically extremes of high temperature (up to 70 ^{o}C) and wide pH variations (2.0 ~ 10.0).[4,5] Ferritin protein has hydrophobic and hydrophilic molecular channels through the protein shell, which enables the removal of the inorganic phase *in vitro* by reductive dissolution. The reconstitution of ferrihydrite cores into a ferritin protein cage proceeds through remineralization of apoferritin by Fe^{2+} oxidation, usually by O_2. A synthesis of ferrimagnetic ferritin (γ-Fe_2O_3) was prepared by a chemical remineralization procedure[6,7] with the assistance of H_2O_2 oxidant in 3-[(1,1-dimethyl-2-hydroxyethyl)amino]-2-hydroxy-propanesulfonic acid (AMPSO) buffer (pH 8.5) at 65 ^{o}C under N_2 gas. Biomineralization of other metals (*i.e.*, Co,[8] Mn,[9-11] and Ni[12]) or semiconductors (CdS)[13] into the ferritin cavity has also been reported. Wong *et al*. demonstrated the magnetic transition from superparamagnetic to ferromagnetic CoPt cored ferritin.[14,15] Tetrachloroplatinated anion was moved to the ferritin core and fabricated to Pt nanoparticles by chemical reduction. The electrochemical behavior of the physically-adsorbed ferritin molecules on indium-tin oxide (ITO) glass was studied via cyclic voltammetry.[16,17] The ferritin was well adsorbed onto ITO substrate from solution at a controlled electrode potential and could be electrochemically induced to release the iron core without the need for a reducing agent.

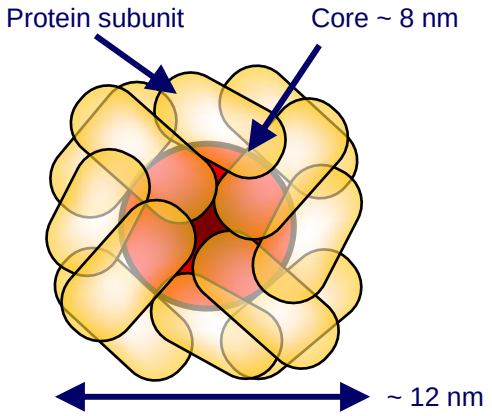

Figure 1. Schematic of the spherical shell of the ferritin protein.

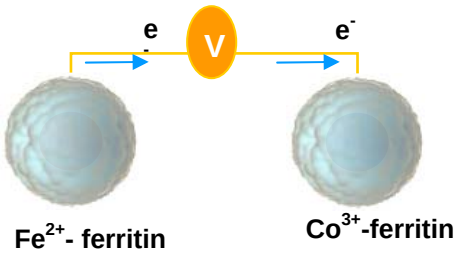

$$Fe(OH)_3 + e^- \leftrightarrow Fe(OH)_2 + OH^- \quad E^o = -0.49V$$

$Fe(OH)_3/Fe(OH)_2$ II $CoOOH/Co(OH)_2$ E_{cell} = 0.66 V
$Fe(OH)_3/Fe(OH)_2$ II γ-$MnOOH/Mn(OH)_2$ E_{cell} = 0.20 V
$Fe(OH)_3/Fe(OH)_2$ II $NiOOH/Ni(OH)_2$ E_{cell} = 0.97 V

Figure 2. Schematic of the bio-nanobattery concept. The redox potential difference between ferritins with different core materials produces the electron transfer from a donor to an acceptor.

As one application area of bioinorganic molecules, bionanobattery concept is based on ferritin protein to store energy.[18-20] By reconstitution process of site-specific biomineralization within the protein cage, ferritins are loaded with different core materials such as Co,[8] Mn,[9-11] Ni,[12] Pt,[21] etc. Each of the core material has a different redox potential and can be fabricated into 2-D arrays for a high energy capacity. The bionanobattery consists of two ferritin half-cell units with a different redox potential between them (see Fig. 2). As another application area, direct energy harvesting[22-25] is an excellent strategy provided that sufficient power is available without having to enlarge the system significantly. The biofuel cells, functioning as an energy conversion device, is based on the ferritin reconstituted and/or combined other biomolecules to generate the power.[26,27]

In this work, an electrochemically-controlled, site-specific biomineralization was demonstrated through the immobilization of biomolecules on a substrate to produce the biologically-derived nanoparticle array. The electrode surface was modified to ensure a strong and stable adhesion of ferritin molecules and to reconstitute the core material with another metal. We used the electrochemical biomineralization technique for the direct reconstitution of immobilized ferritins on a gold electrode. We also demonstrated the electrochemical behaviors of reconstituted ferritin electrodes for bioelectronics applications.

EXPERIMENTAL

Chemical Reconstitution of Ferritin. Apo ferritin was prepared by the reductive dissolution of native iron oxide cores of holo horse spleen ferritin (HoSF, Sigma) using the thioglycollic acid procedure.[28] Apo HoSF was further reacted with dithionite in the presence of bipyridine to remove iron. Protein concentrations were determined by the Lowry method and confirmed by the absorbance at 280 nm which is a specific amino acid absorption peak.[29] Co and Mn oxyhydroxide mineral cores were fabricated within the ferritin interior.[30,31] Apoferritin solution prepared in the above procedure was adjusted to a proper pH level with 0.01 M NaOH. $Co(NO_3)_2$ (25 mM, 80 μl) was used as a cobalt source and added to apoferritin solution, followed by addition of excess amount of H_2O_2 (3 vol.%, 40 μl). Co addition was conducted over 2 hr period with 10 min intervals, maximizing metal loading. Just before Co ferritin started to precipitate due to excess Co loading, the reconstitution reaction was stopped by adding 3 μl of catalase. In this work, the amount of Co loading was measured to be 1600 Co per ferritin molecule. According to spectroscopy results, Co atoms loaded inside ferritin exist as Co(III)-oxyhydroxide, CoOOH.[8] Higher Co loadings can be attained but the reaction becomes slow and the yield decreases because of protein precipitation as the core approaches its theoretical limit of 4000 Co per ferritin. This ferritin reconstitution can be basically applied to any other metal loadings. Manganese also can be reconstituted in the cavity as manganese oxyhydroxide (MnOOH) by natural oxidation. Also, nickel can be fabricated as nickel hydroxide ($Ni(OH)_2$) during the hydroxylation process of nickel ion solution that requires dissolved CO_2 and a precise pH control.[12]

Electrochemical Reconstitution of Ferritin. Immobilization of ferritins on a Au electrode is achieved by the self-assembly methods based on DTSP and alkanethiols. The Fe-core inside ferritin is removed during a potential sweep at a given potential that is higher than the Fe(III) reduction potential in the presence of chelating agents such as bipyridine

(bipy, Aldrich, 99 %) and ethylenediaminetetraacetic acid (EDTA, Aldrich, 99 %) bisodium salt. The ferritin-immobilized Au electrode was prepared following the ferritin immobilization procedure. A cleaned Au electrode was inserted into the DTSP and mercaptopropanol (MPOH) solutions for 1 hr and then washed with acetone and HEPES buffer in succession. The mixed self-assembled monolayer (SAM)-modified Au electrode was immersed into the ferritin solution for 18 hr at 4 ^{o}C to produce the ferritin immobilized Au electrode. This electrochemical removal of metal core with chelating agents produces the analogous product of immobilized apoferritins on DTSP-modified Au electrodes. The electrochemical biomineralization of ferritins is accomplished by a potential sweep or a constant potential step with a more negative potential than the metal ion reduction potential in metal ion solutions. Electrochemical biomineralization of the immobilized ferritins was carried out in a 0.05 M phosphate buffer (pH 7.5) solution containing a chelating agent of EDTA at room temperature. The immobilized apoferritin was immersed into a solution with the volume ratio of 3 to 1 of 0.05 M HEPES buffer (0.05 M) and $(NH_4)_2PtCl_4$ (0.05 M) for 30 min. Platinum anions likely entered the ferritin through the channels in the protein shell. The apoferritin containing platinum ion was washed with 0.025 M HEPES buffer several times and inserted into 0.05 M phosphate buffer again. Platinum ion is electrochemically reduced to pure platinum through the potential cycling to more negative potential than that of platinum ion reduction. Through the repetition of this process, we can increase the number of atoms inside the ferritin. Using this method, we can control the number of metal atoms deposited inside the ferritin by controlling the total charge passed and the valance of the target metal is determined by the electrolyte pH and the engaged potentials. In addition, this procedure allows for the electrochemical biomineralization with various metals and an easy reconstitution without maintaining the stringent conditions of an anaerobic environment with a precise control of pH and temperature.

Electrochemical Measurements and Microscopic Analysis. Electrochemical measurements of immobilized ferritins were carried out in a 0.05 M phosphate buffer (pH 7.5) solution either with or without a chelating agent of EDTA at room temperature. Cyclic voltammograms (CVs) were recorded using an EG&G PAR 273A potentiostat/galvanostat controlled by Power Suites software. Quartz crystal microbalance (QCM) and electrochemical QCM measurements were performed using QCA 922A (EG&G) operated by WinEchem software. For QCA/EQCM analysis, gold-plated quartz electrodes (9 MHz AT-cut) were cleaned with doubly distilled, deionized water followed by immersing in a piranha solution. An increase in mass corresponds to decrease in frequency according to the Sauerbrey equation: [32]

$$\Delta m = - C_f \cdot \Delta f$$

Where, Δm is the mass change, Δf is the change in frequency, and C_f is the sensitivity constant (here, C_f is 1.068 ng/Hz). Each solution was purged with nitrogen for 10 min before the acquisition of the electrochemical measurements. Gold on silicone wafer (Platypus Technologies, 100 nm gold thickness) electrode was prepared as working electrode, according to the above immobilization methods. The Ag/AgCl (in 3 M NaCl) electrode was used as reference electrode. The counter electrode was a spiral platinum wire. Field emission-scanning electron microscopy (FE-SEM) was carried out on a Hitachi S-5200 on the immobilized ferritin layers and the reconstituted ferritins. The immobilized ferritins layer was thoroughly rinsed with 25 mM HEPES buffer and doubly distilled, deionized water, dried in a nitrogen atmosphere, and then subjected to the microscopic analysis.

RESULTS AND DISCUSSION

Electrochemical Behaviors of Chemically-Reconstituted Ferritin. A cleaned Au electrode was inserted into the DTSP and MPOH solutions for 1 hr and then washed with acetone and HEPES buffer in succession. The mixed SAM-modified Au electrode was immersed into the ferritin solution for 18 hr at 4 ^{o}C to produce the ferritin immobilized Au electrode. The topography and electrochemical behavior of this electrode are shown in Fig. 3a and b, respectively. The electron transfer between the ferritin core metals and the substrate occurred easily on the immobilized ferritin electrode. The reduction of Fe(III) occurred at – 0.65 V gradually and then the current decreased depending on the number of cycles but the oxidation of Fe(II) was not observed in the reverse potential scan. The CVs are consistent with the fact that although Fe(II) is soluble in phosphate buffer, Fe(III) is not. This difference in solubility is particularly apparent when Fe(II) solutions are exposed to air. The rapid oxidation of Fe(II) to Fe(III) occurs at pH 7 forming a white precipitate of $FePO_4$ within a few seconds, since the phosphate anions have a strong affinity for iron oxyhydroxide.[33] The ratio of phosphate to iron for mammalian ferritin is 10 % with phosphate possibly adsorbed on the surface of the iron oxyhydroxide. Thus, the reduced Fe(II) ions are released to the solution as free Fe(II) ions, followed by a reaction with phosphate ions to form the $FePO_4$ precipitate upon oxidation. Therefore, the oxidation current of Fe(II) is not reversible for the reverse scan. A new cathodic peak grew at – 0.4 V as the cycling repeated. This faradaic reaction is likely caused by the reduction of accumulated and/or diffused $FePO_4$ precipitate onto the substrate. Figure 3c shows the frequency changes accompanying with potential cycling recorded at 10 mV/s in 0.05 M phosphate buffer (pH 7.5) to measure the number of Fe atom releases outside the ferritin protein shell during cycles. The Fe(II) release starts to reverse scan except fist scan. It indicates the rate of iron release from ferritin inside is slow process due to the passing through the protein shell. The frequency changes

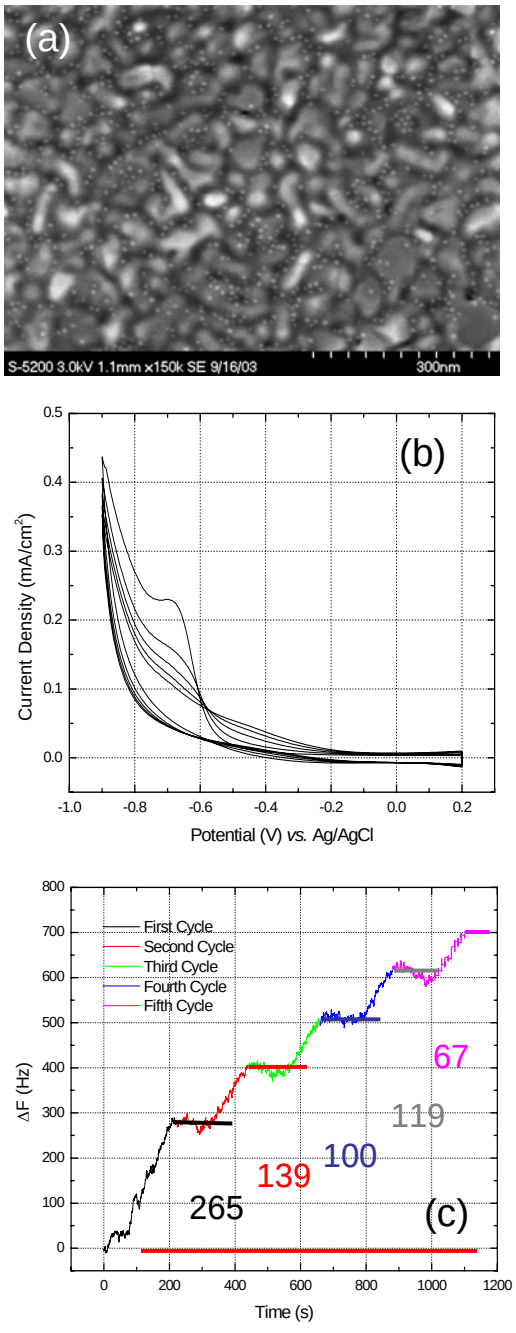

Figure 3. (a) FE-SEM image, (b) CVs, and (c) EQCM data of immoblilized ferritin on DTSP and MPOH-modified Au electrode in 0.05 M phosphate buffer (pH 7.5).

recorded during each cycle on the immobilized ferritin electrode were + 265, + 139, + 100, + 119, and + 67, respectively, for the Fe(II) release. This tendency is exactly the same as that shown by the CV results (see Fig. 3b) to reduce the cathodic current density depending on cycles, indicating that the reduced Fe(II) is released into the solution. During the forward scan, the frequency increase is due to the proton insertion and precipitation of $FePO_4$ made by combination of reduced Fe(II) and phosphate ions on electrode surface. We measured the number of ferritins immobilized on DTSP and MPOH-modified Au electrode is 6.59×10^{12} from QCA data (not shown here). Based on the number of ferritins on Au electrode, the total number of Fe release from one ferritin is 1206, indicating that the iron is releasing more than 50 % of normal number (= 2000) of Fe in a ferritin for the first five cycles.

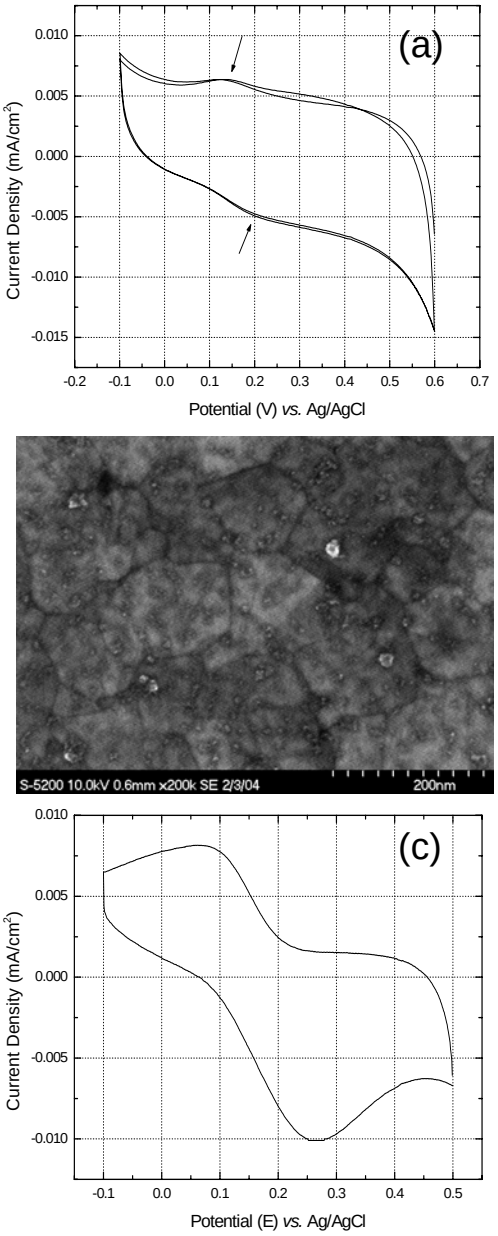

Figure 4. (a) CV of physically adsorbed Co-cored ferritin in 0.05 M phosphate buffer (pH 7.5). (b) FE-SEM image and (c) CV of immobilized Co-cored ferritin on DTSP and MPOH-modified Au electrode in 0.05 M phosphate buffer (pH 7.5).

The iron-core inside ferritin was replaced with cobalt through the above procedure with the aid of H_2O_2 oxidant. Au electrode was cleaned chemically before inserted in the MOPS buffer solutions containing Co-cored ferritin (0.5 mg/ml) for 18 hr. Figure 4a shows the current-voltage curve of physically-adsorbed Co-cored ferritin on Au electrode in 0.05 M phosphate buffer at pH 7.5. The peak at 0.15 V represents the reduction of the physically-adsorbed Co-cored ferritin layer. It is not induced from reduction of free Co ions in the ferritin reconstitution sample because the free Co ions were removed when the sample was passed through a G-25 Sephadex column. The redox pair of cobalt around 0.15 V is induced from reduction of CoOOH to $Co(OH)_2$ and the corresponding oxidation for the reverse scan. This reaction was so reversible that the phosphate buffer did not affect it. In spite of the large population of ferritin on the substrate, the current signal of Co-cored ferritin layer is small due to the small number of cobalt metal atoms inside ferritin molecule. The topography and electrochemical behavior of immobilized Co-cored ferritin on DTSP and MPOH-modified Au electrode are shown in Fig. 4b and c, respectively. The ferritin population in spite of the low concentration of ferritin is similar with one of Fe-cored ferritin. It shows well-dispersed Co-cored

ferritin on Au electrode. The capacitive current of immobilized Co-cored ferritin electrode is smaller than that of physically-adsorbed ferritin layer due to the surface modification with SAM. The cathodic and anodic peaks of cobalt clearly show at 0.08 and 0.26 V, respectively. The increased overpotential on the immobilized Co-cored ferritin is about 70 mV on both the anodic and the cathodic reactions due to the surface modification using DTSP.

We measured the electrochemical behaviors of Mn-cored ferritin reconstituted by natural oxidation. Figure 5a shows a FE-SEM image of physically adsorbed Mn-cored ferritin on Au electrode. The cleaned Au electrode was immersed in the MOPS buffer solution containing Mn-cored ferritin at a concentration of 2 mg/ml for 18 hr. Although Mn-cored ferritin has a higher concentration than Co-cored ferritin, the population of Mn-cored ferritin on Au was not higher. Mn(IV) is an important candidate material mainly as electrolytic manganese dioxide is an excellent cathode material for high performance batteries.[34,35] The electrochemical oxidation of manganese is very complicated since its oxidation produces different products with their oxidation states between Mn(II) and Mn(VII) depending on experimental condition. The oxidation of manganese in alkaline media is described as consisting of a number of steps: $Mn(OH)_2$ is produced at a low applied potential and higher oxidized states are obtained at more positive potentials. CVs were recorded during the two cycles of physically-adsorbed Mn-cored ferritin on Au in 0.05 M phosphate buffer with different pH as shown in Figure 5b. There were two cathodic peaks and two anodic peaks during potential sweep. For the first cycle, the cathodic peak at 0.25 V did not appear because manganese was present at three valence states inside ferritin. First, MnOOH is reduced to the $Mn(OH)_2$ at - 0.2 V and Mn(II) is oxidized to Mn(III) at 0.1 V. Generally, anodic counterpart of cathodic peak at -0.2 V is not identified in CVs in high pH solutions. In our case, we can see the shoulder-like small peak at 0.1 V (pH 9.0) and 0.3 V (pH 7.5) in weakly basic media. The large anodic peak results from oxidation to higher valence oxides inside ferritin. The large cathodic peak corresponds to the reduction of anodic reaction products at 0.75 V. This oxide layer

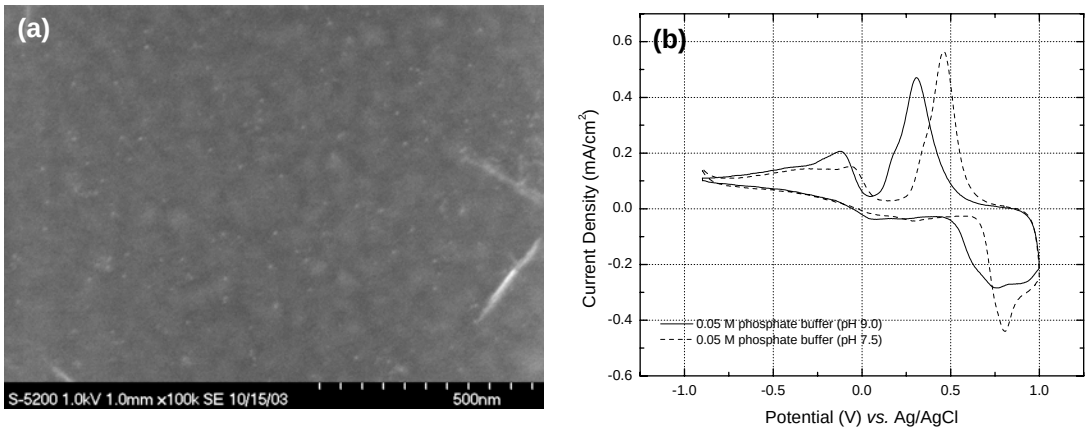

Figure 5. (a) FE-SEM image and (b) CVs of physically adsorbed Mn-cored ferritin in 0.05 M phosphate buffer (pH 7.5).

seems to be made of MnO_2, hydroxide, and/or mixed oxides such as $MnO_x(OH)_y$, because it results from oxidation of $Mn(OH)_2$ and/or MnOOH. For the bionanobattery application with Mn-cored ferritin, we have to change the ionic state of manganese from + 3 to + 4 chemically or electrochemically for gaining the higher cell potential because the

chemically self-fabricated ferritins composed of MnOOH.[9-11] Mn-cored ferritin used as a cathode has to be oxidized to higher oxidation state because the redox couple of Mn(II)/Mn(III) has a low equilibrium potential and the oxidation of Mn(II) can not be observed.

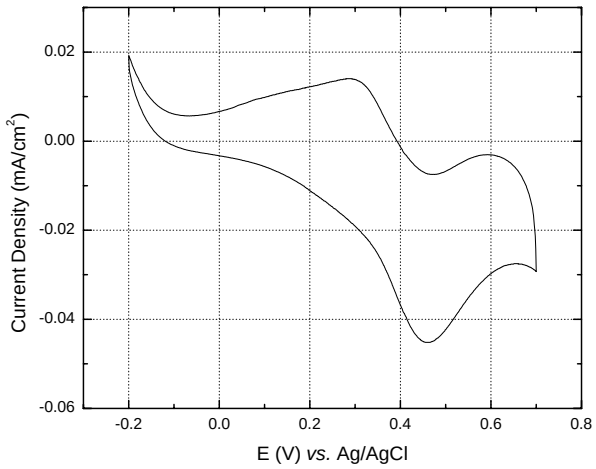

Figure 6. CV of physically adsorbed Ni-cored ferritin on Au electrode in 0.05 M phosphate buffer (pH 7.5) at a scan rate of 100 mV/s.

A redox couple of nickel, i.e., nickel hydroxide ($Ni(OH)_2$) and nickel oxyhydroxide (NiOOH), was shown to be involved in the oxidation of nickel oxides in phosphate buffer. Nickel is known to have oxidation states of Ni(0), Ni(II), Ni(III), and Ni(IV) in alkaline media. The first step of nickel oxidation is from Ni(0) to α-$Ni(OH)_2$. α-$Ni(OH)_2$ is slowly changed to β-$Ni(OH)_2$, which passivates the nickel electrode surface. β-$Ni(OH)_2$ thus produced cannot be reduced to Ni(0). The α- and β-$Ni(OH)_2$ are further oxidized to γ- and β-phases of nickel oxides of higher valences, respectively.[36,37] These oxides and oxyhydroxides are believed to have mixed stoichiometries rather than a definite oxidation state. Figure 6 shows the cyclic voltammograms of a physically-adsorbed Ni-cored ferritin in 0.05 M phosphate buffer (pH 7.5) at scan rate of 100 mV/s. The cyclic voltammograms are in good agreement with those reported in the literature in the potential region that is of interest in this study.[36,37] In the case of Ni-cored ferritin, the state of nickel in the self-fabricated ferritin is not known accurately yet.[12] If the valence state of nickel prepared by the self-fabrication is Ni(III), *i.e.*, NiOOH, the expected cell potential can be higher, *i.e.*, 0.97 V (*vs.* NHE) in the bionanobattery application with $Fe(OH)_2$-NiOOH pair. The capacity of bionanobattery depends on the population of ferritin and the number of metal atoms in ferritin cavity. In terms of battery performance, multi-stacking of ferritin layers can be an important way to increase the number of ferritin molecules on Au electrode.

Electrochemical Site-Specific Reconstitution of Ferritin. An apoferritin was immobilized onto the DTSP and MPOH-modified Au electrode. The faradaic reaction on the apoferritin immobilized Au electrode did not occur in the potential region of 0.7 to – 0.6 V as shown in Fig. 7a. The reduction of the remaining Fe(III) inside the ferritin for the removal of metal core occurs at – 0.7 V with a small shoulder. After platinum ion addition into the apoferritin, platinum ion is reduced through the potential sweep from 0.2 to – 1.0 V. The CV of platinum reconstituted ferritin in 0.05 M phosphate buffer (pH 7.5) is shown in Fig. 7b. New reduction and oxidation peaks were induced from Pt metal in the phosphate buffer. Two reduction and the corresponding oxidation peaks at a more negative potential than – 0.5 V are likely due to the phosphate ion reduction and oxidation. The reduction of platinum oxide and gold oxide occurred at – 0.1 and 0.4 V, respectively. Each peak current induced from Pt increases depending on the number of dipping cycles. On the other hand, the reduction process of gold oxide at 0.4 V decreased due to the

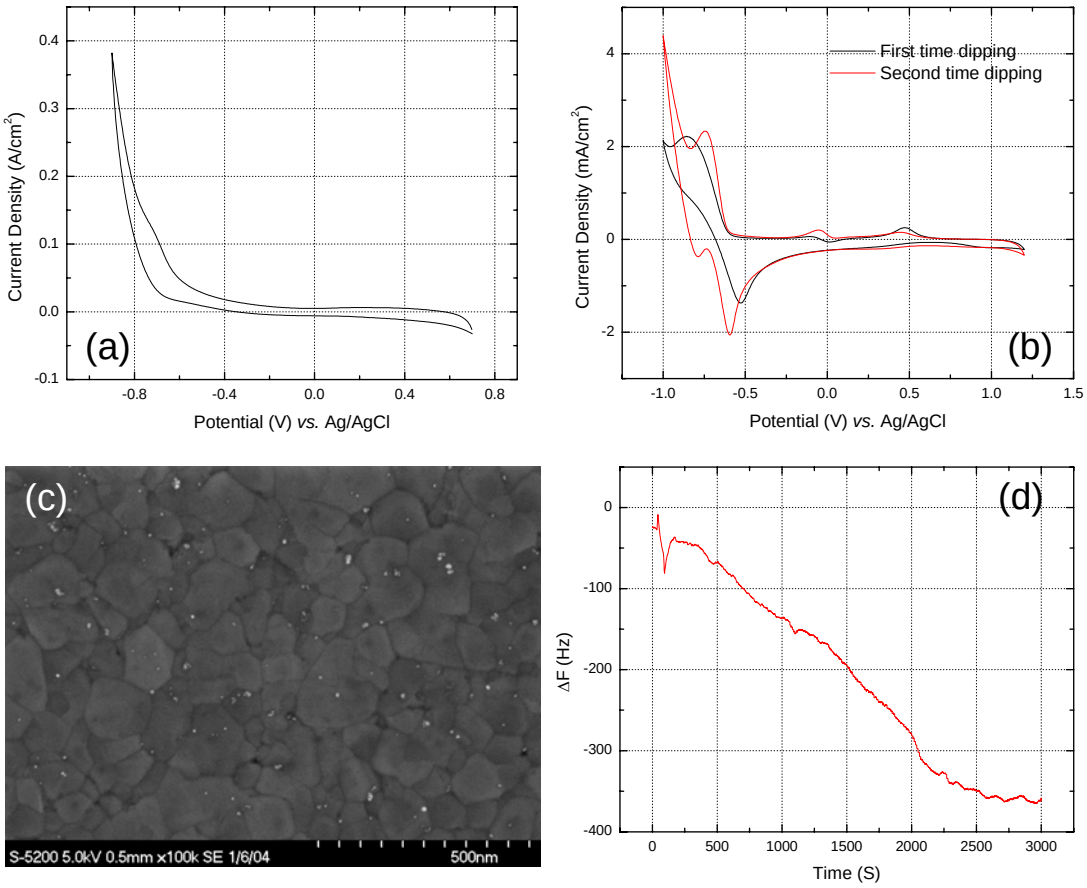

Figure 7. (a) CV of immobilized apoferritin on DTSP and MPOH-modified Au electrode in 0.05 M phosphate buffer (pH 7.5). (b) CVs of platinum reconstituted ferritin in 0.05 M phosphate buffer for first and second dipping process. (c) FE-SEM image of Pt-cored ferritin fabricated by electrochemical site-specific reconstitution using the DTSP and MPOH-modified Au electrode. (d) Frequency decrease upon addition of platinum ions such that its final volume ratio of HEPES buffer (0.05 M) to platinum ions (0.05 M) would becomes 3 to 1. The experiment was performed at open circuit potential.

increased amount of platinum inside the ferritin. Figure 7c shows FE-SEM image of Pt-cored ferritin fabricated by electrochemical site-specific reconstitution of ferritin using mixed SAM-modified Au electrodes. The reconstituted Pt-cored ferritin is well-isolated and dispersed across the entire electrode. The size of Pt-cored ferritin is slightly smaller than theoretical because the ferritin size depends on the number of metal atoms inside the ferritin protein shell. The frequency changes recorded during insertion of platinum ions into the ferritin were about + 364 Hz for 3000 sec (see Fig. 7d). Based on the number of apoferritins on Au electrode (5.49×10^{12} from QCA data (not shown here)), the total number of inserted platinum ion inside a ferritin is around 127 due to the large size of $PtCl_4^{2-}$. The electrocatalytic activity for oxygen reduction was evaluated with the electrochemically site-specific reconstituted Pt-cored ferritin on a Au electrode. Figure 8 shows the linear sweep voltammograms (LSVs) for oxygen reduction at a bulk platinum electrode and reconstituted Pt-cored ferritins immobilized on the Au electrodes through various surface treatments in 0.05 M phosphate buffer (pH 7.5) saturated with oxygen. The Pt-cored ferritins used were electrochemically site-specific biomineralized on a Au electrode inserted into the $PtCl_4^{2-}$ solution for 30 min. In the 10^{th} sweep, oxygen reduction on the Pt starts from 0.1 and 0.3 V on Pt-cored ferritin and bulk Pt, respectively. The reduc-

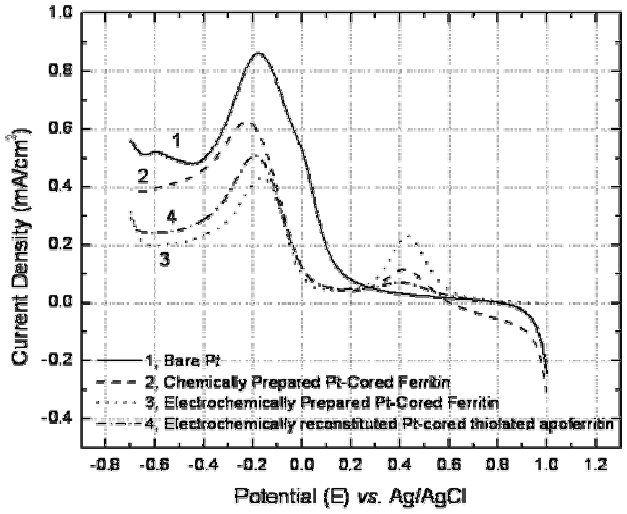

Figure 8. LSVs of bulk Pt (line 1) and Pt-cored ferritin (lines 2, 3, and 4) in 0.05 M phosphate buffer (pH 7.5) with saturated oxygen. The scan rate was 100 mV/s.

tion peak around 0.4 V is induced from gold oxide reduction. The current density of gold oxide reduction at each electrode depends on the surface coverage of Pt-cored ferritin on the Au electrode. The thiolated ferritin SAM forms the highest populated film among these surface treatments. The rising slope in current is similar at the Pt-cored ferritin electrodes, indicating that the oxygen reduction kinetics is almost identical without regard to the preparation methods. The cathodic currents were limited due to the diffusion process of oxygen through the protein shell. The cathodic current density at the chemically prepared Pt-cored ferritin electrode is the highest for oxygen reduction among the Pt-cored ferritin electrodes due to the population and number of Pt atoms inside the ferritin. It is important to note that the amount of Pt in the Pt-cored ferritin electrode is much smaller than bulk Pt at the same geometric electrode area. The surface coverage and the number of Pt atoms in the electrode unit area are much smaller than those of bulk Pt, but the current density of electrochemically prepared Pt-cored ferritin represents only half of bulk Pt electrode. Estimation of the amount of Pt on the electrode is not quantitative, but is roughly 6 % through the EDS analysis on the chemically prepared Pt-cored ferritins (not shown here). This indicates that the catalytic activity of the ferritin-stabilized platinum nanoparticles is enhanced by the large surface area and particle size phenomena. The results shown here were reproducible even after the electrode was left exposed to the air for a several days. The nano-sized platinum-cored ferritins on gold are candidate a good catalyst for the electrochemical reduction of oxygen, which is applicable to biofuel cell applications. This results in a smaller catalyst loading on the electrodes for fuel cells or other bioelectronic devices.

CONCLUSION

The ferritin protein has hydrophobic and hydrophilic molecular channels within the protein shell, which makes it possible to remove and insert new inorganic phases. By reconstitution process of site-specific biomineralization within the protein cage, ferritin can be loaded with Co, Mn, and Ni. They showed good electrochemical behaviors for the electron transport. Also, platinum anion coordinated with chloride ions enters the ferritin interior through these channels. Therefore, we can easily modify the electrode surface using immobilization and electrochemical biomineralization methods with various metal ion solutions without complicated chemical treatment such as extraction, dialysis, and column treatment for removing the unbound metal ions. In addition, the catalytic activity of the nanostructured platinum nanoparticles stabilized with ferritin biomolecules is en-

hanced by the large surface area and particle size effects. This first demonstration of electrochemical site-specific reconstitution of biomolecules provides a new tool for biomineralization and opens the way to fabricate the biologically derived nanoparticle arrays. This method may open up numerous possibilities for practical applications of immobilized ferritins such as high-density data storage devices, bioelectronic devices, and biosensors.

REFERENCES

1. Bioastronautics Critical Path Roadmap (BCPR), Office of Bioastronautics, NASA, JSC 62577, April 2 (2004).
2. R. J. White and M. Averner, *Nature*, **409**, 1115 (2001).
3. P. M. Harrison and P. Arosio, *Biochim. Biophys. Acta*, **1275**, 161 (1996).
4. T. Douglas, in *Biomimetic Approaches in Materials Science*, S. Mann, Editor, p. 91, VCH Publishers, New York (1996).
5. G. D. Watt, P. B. Frankel, and G. C. Papaefthymiou, *Proc. Nat. Acad. Sci. USA*, **82**, 3640 (1985).
6. F. C. Meldrum, B. R. Heywood, and S. Mann, *Science*, **257**, 511 (1992).
7. K. K. W. Wong, T. Douglas, S. Gider, D. D. Awschalom, and S. Mann, *Chem. Mater.*, **10**, 279 (1998).
8. T. Douglas and V. T. Stark, *Inorg. Chem.*, **39**, 1828 (2000).
9. F. C. Meldrum, V. J. Wade, D. L. Nimmo, B. R. Heywood, and S. Mann, *Nature*, **349**, 684 (1991).
10. P. Mackle, J. M. Charnock, C. D. Garner, F. C. Meldrum, and S. Mann, *J. Am. Chem. Soc.*, **115**, 8471 (1993).
11. F. C. Meldrum, T. Douglas, S. Levi, P. Arosio, and S. Mann, *J. Inorg. Biochem.*, **58**, 59 (1995).
12. M. Okuda, K. Iwahori, I. Yamashita, and H. Yoshimura, *Biotechnol. Bioeng.*, **84**, 187 (2003).
13. K. K. W. Wong and S. Mann, *Adv. Mater.*, **8**, 928 (1996).
14. B. Warne, O. I. Kasyutich, E. L. Mayes, J. A. L. Wiggins, and K. K. W. Wong, *IEEE Trans. Magnet.*, **36**, 3009 (2000).
15. E. L. Mayes, A. Bewick, D. Gleeson, J. Hoinville, R. Jones, O. I. Kasyutich, A. Nartowski, B. Warne, J. A. L. Wiggins, and K. K. W. Wong, *IEEE Trans. Magnet.*, **39**, 624 (2003).
16. R. J. Cherry, A. J. Bjornsen, and D. C. Zapien, *Langmuir*, **14**, 1971 (1998).
17. K. C. Martin, S. M. Villano, P. R. McCurdy, and D. C. Zapien, *Langmuir*, **19**, 5808 (2003).
18. G. C. King, S.-H. Chu, J.-W. Kim, Y. Park, P. T. Lillehei, S. H. Choi, G. D. Watt, R. C. Davis, and J. N. Harb, in *Smart Structures and Materials/2004*, V. K. Varadan, Editor, PV 5389, p 461, Proceedings of SPIE, Bellingham, WA (2004).
19. G. D. Watt, NASA Invention Disclosure, Case #LAR 16640-1 (2003).
20. J.-W. Kim, S. H. Choi, S.-H. Chu, Y. Park, G. C. King, and J. R. Elliott, NASA Invention Disclosure, Case #LAR 17008-1 (2004).
21. J.-W. Kim, S. H. Choi, P. T. Lillehei, G. C. King, S.-H. Chu, G. D. Watt, Y. Park, *Chem. Mater.*, To be submitted (2004).
22. T. Chen, S. C. Barton, G. Binyamin, Z. Gao, Y. Zhang, H.-H. Kim, and A. Heller, *J. Am. Chem. Soc.*, **123**, 8630 (2001).
23. T. Ikeda and K. Kano, *J. Biosen. Bioengineer.*, **92**, 9 (2001).

24. N. Man, F. Mao, and A. Heller, *J. Am. Chem. Soc.*, **125**, 6588 (2003).
25. E. Katz and I. Willner, *J. Am. Chem. Soc.*, **125**, 6803 (2003).
26. J.-W. Kim, P. T. Lillehei, G. D. Watt, S. H. Choi, S.-H. Chu, Y. Park, and G. C. King, NASA Invention Disclosure, Case #LAR 16758-1 (2003).
27. J.-W. Kim, S. H. Choi, P. T. Lillehei, G. C. King, G. D. Watt, S.-H. Chu, Y. Park, and S. Thibeault, in *Smart Structures and Materials/2004*, V. K. Varadan, Editor, PV 5389, p 452, Proceedings of SPIE, Bellingham, WA (2004).
28. A. Treffry and P. M. Harrison, *Biochem. J.*, **171**, 313 (1978).
29. G. Zhao, F. Bou-Abdallah, X. Yang, P. Arosio, and D. Chasteen, *Biochemistry*, **40**, 10832 (2001).
30. B. Zhang, S.-H. Chu, S. H. Choi, J.-W. Kim, J. H. Harb, R. C. Davis, and G. D. Watt, *Inorg. Chem.*, Under revision (2004).
31. B. Zhang, J. H. Harb, R. C. Davis, S.-H. Chu, S. H. Choi, J.-W. Kim, and G. D. Watt, *Inorg. Chem.*, Under revision (2004).
32. M. D. Ward, in *Physical Electrochemistry*, I. Rubinstein, Edit, Marcel Dekker, New York (1995).
33. Y. G. Cheng and N. D. Chasteen, *Biochemistry*, **30**, 2947 (1991).
34. B. D. Desai, J. B. Fernandes, and V. N. Kamat Dalal, *J. Power Sources*, **16**, 1 (1985).
35. L. Bai, D. Y. Qu, B. E. Conway, Y. H. Zhou, G. Chowdhury, and W. A. Adams, *J. Electrochem. Soc.*, **140**, 884 (1993).
36. C. Zhang and S.-M. Park, *J. Electrochem. Soc.*, **136**, 3333 (1989).
37. J.-W. Kim and S.-M. Park, *J. Electrochem. Soc.*, **146**, 1075 (1999).